Effect of Doping Profile Variation on GaAs Hybrid and Double-Read IMPATT Diode Performance at 60 and 94 GHz

MOUSTAFA A. EL-GABALY, SENIOR MEMBER, IEEE, RICHARD K. MAINS, MEMBER, IEEE, AND GEORGE I. HADDAD, FELLOW, IEEE

Abstract—**Doping profile parameters were varied in a computer optimization of hybrid and double-read GaAs IMPATT diodes at 60 and 94 GHz. The energy-momentum transport model was used to simulate each structure. Optimum results for the various structures that were studied are presented and compared.**

I. INTRODUCTION

THE INCLUSION of energy and momentum relaxation effects significantly changes the predicted performance and design criteria of millimeter-wave GaAs IMPATT's from that predicted by the drift-diffusion model [1], [2]. In particular, the optimum drift lengths are found to be shorter when energy and momentum relaxation effects are included [3].

In this paper, double-read doping profiles based on previous energy-momentum simulation results are used as starting points for the computer optimization; the drift lengths and integrated charge of the doping spikes are then varied and the effect on diode performance at 60 and 94 GHz is presented. Also, for hybrid structures, the effects of varying the drift lengths and doping levels are given.

II. RESULTS AT 60 GHZ

Fig. 1(a) shows the general doping profile configuration for all the double-read structures examined. Q_p and Q_n are the integrated charges in the doping spikes which border the high-field region, given in units of cm^{-2} in the tables. These doping spikes are 0.04 μm wide for all the double-read profiles. The drift lengths l_n and l_p are measured to the center of the doping spikes. The p-n junction is located midway between the doping spikes.

Fig. 1(b) shows the doping profile configuration for the hybrid structures that were studied. The junction is located between the uniformly doped p-type layer with doping N_A and the highly doped n-type region of value N_D^H. N_D is the doping level in the n-drift region of length l_n.

Table I presents the optimum efficiencies obtained for three double-read structures at 60 GHz. The dc solution

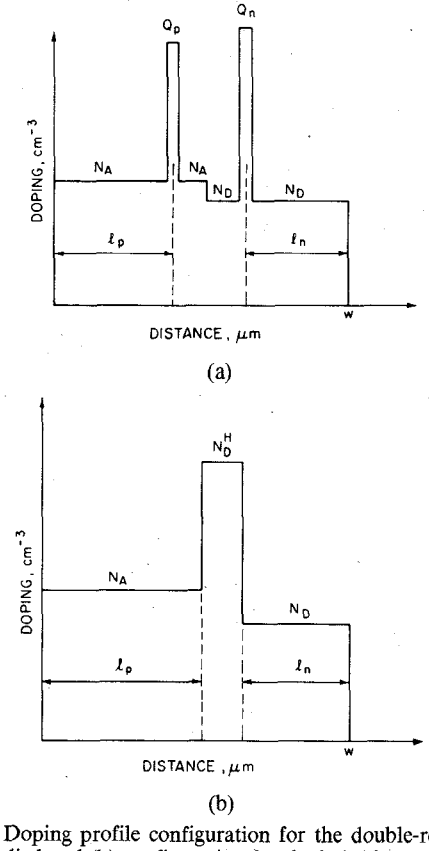

Fig. 1. (a) Doping profile configuration for the double-read structures studied and (b) configuration for the hybrid structures.

for DR1, the starting structure, is shown in Fig. 2(a) and for DR3 in Fig. 2(b). The solid line in this figure is the electric field which is positive to the left. The plus and minus signs represent the hole and electron particle currents, respectively. Since Q_p is considerably smaller than Q_n for this structure, the electric field is higher on the p-side than on the n-side. The optimum efficiency obtained for this structure was 16.6 percent.

The structure DR2 of Table I is similar to structure DR1 except that the doping spikes Q_n and Q_p were changed to raise the electric field on the n-side and to lower the field on the p-side, so that on both sides the electric field in the drift region immediately adjacent to the doping spike is approximately 2.8×10^5 V/cm. Raising the field on the n-side allows a larger voltage modulation (V_{RF}/V_{op}), 0.729

Manuscript received December 19, 1983; revised April 2, 1984. This work was supported by the Air Force Systems Command, Avionics Laboratory, Wright-Patterson Air Force Base, OH, under Contract F33615-81-K-1429.

The authors are with the Solid-State Electronics Laboratory, Department of Electrical and Computer Engineering, University of Michigan, Ann Arbor, MI 48109.

0018-9480/84/1000-1342$01.00 ©1984 IEEE

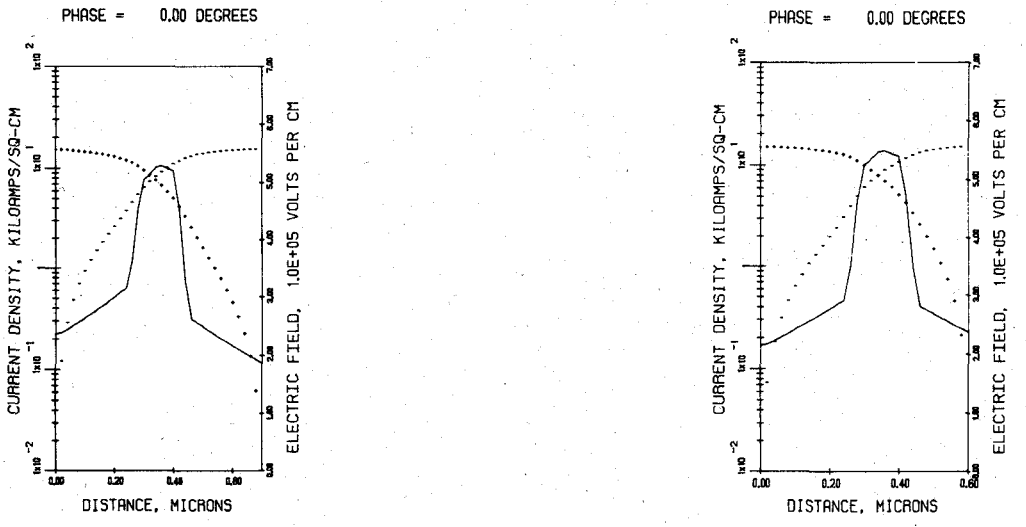

Fig. 2. (a) DC solution for structure DR1 of Table I ($J_{dc}=15.0$ kA/cm^2, $T=500$ K, $V_{dc}=21.84$ V) and (b) dc solution for structure DR3 ($J_{dc}=16.0$ kA/cm^2, $T=500$ K, $V_{dc}=19.89$ V).

TABLE I
LARGE-SIGNAL RESULTS AT 60 GHz FOR DIFFERENT DOUBLE-READ DOPING PROFILE PARAMETERS USING THE ENERGY-MOMENTUM SIMULATION
($N_A=4.0\times10^{16}$ cm^{-3}, $N_D=2.0\times10^{16}$ cm^{-3}, $T=500$ K)

Case No.	ℓ_p (μm)	ℓ_n (μm)	w (μm)	Q_p (10^{12} cm^{-2})	Q_n (10^{12} cm^{-2})	V_{RF} (V)	V_{op} (V)	J_{dc} (kA/cm^2)	η (%)	Y_D (s/cm^2)	P_{RF} (W/cm^2)	P_{RF} (W) (R_D = 1 Ω)	P_{diss} (W) (R_D= 1 Ω)
DR1	0.27	0.27	0.7	1.28	2.4	13.0	21.54	10.12	16.6	- 426.6 + j5724	3.60 x 10^4	0.466	2.35
DR2	0.27	0.27	0.7	1.6	1.8	15.5	21.27	15.28	20.08	- 543.4 + j5629	6.528 x 10^4	1.11	4.41
DR3	0.27	0.17	0.6	1.6	1.8	14.5	20.45	15.0	22.0	- 642 + j6447	6.75 x 10^4	1.04	3.66

TABLE II
LARGE-SIGNAL RESULTS VERSUS J_{dc} FOR STRUCTURE DR1 OF TABLE I
($f=60$ GHz, $T=500$ K)

J_{dc} (kA/cm^2)	$-G_D$ (s/cm^2)	B_D (s/cm^2)	D (1 Ω) (inch)	V_{op} (V)	η (%)	P_{RF} (1 Ω) (W)	P_{diss} (1 Ω) (W)	θ_R (1 Ω) (°C/W)	V_{RF} (V)
10.12	426.6	5724.6	0.0016	21.46	16.6	0.47	2.34	96.1	13
12.28	519.25	5653.2	0.00178	21.55	16.58	0.707	3.56	63.29	13
14.29	595.2	5582.9	0.00193	21.54	16.33	0.95	4.86	46.27	13
16.44	674.6	5503.9	0.00208	21.54	16.1	1.251	6.519	34.51	13
18.47	741.07	5425.1	0.00221	21.50	15.77	1.55	8.27	27.22	13
20.56	805.6	5340	0.00233	21.46	15.42	1.88	10.31	21.82	13
23.85	954.82	5188.8	0.0026	21.65	14.44	2.56	15.00	15.00	12.5
26.87	1031.8	5052.1	0.00277	21.58	13.9	3.13	19.37	11.61	12.5
29.82	1107.7	4914.3	0.00294	21.56	13.46	3.78	24.28	9.27	12.5
32.3	1150.05	4790.0	0.00306	21.47	12.96	4.26	28.60	7.87	12.5

for structure DR2 versus 0.604 for DR1. The optimum large-signal efficiency for DR2 is also increased to 20.08 percent.

To obtain structure DR3, the drift length for electrons was reduced by 0.1 μm, which increased the efficiency to 22.0 percent.

Table II shows the large-signal results versus bias current density J_{dc} obtained for structure DR1. In Table II, P_{RF} is the power that would be obtained if the diode area is chosen so that the diode negative resistance equals 1 Ω. These operating points are not always realizable for CW operation, since the diode may heat excessively at higher

TABLE III
PREDICTED CW PERFORMANCE OF STRUCTURE DR1 OF TABLE I
TAKING INTO ACCOUNT THERMAL LIMITATIONS
($f = 60$ GHz)

J_{dc} (kA/cm^2)	CM D (inch) θ ($^\circ$C/W) P_{RF} (W)	CM R_c (Ω)	DM D (inch) θ ($^\circ$C/W) P_{RF} (W)	DM R_c (Ω)	CR D (inch) θ ($^\circ$C/W) P_{RF} (W)	CR R_c (Ω)	DR D (inch) θ ($^\circ$C/W) P_{RF} (W)	DR R_c (Ω)
12.28	0.00178 63.3 0.707	1.00 E	0.00178 63.3 0.707	1.00 E	0.00178 63.3 0.707	1.00 E	0.00178 63.3 0.707	1.00 E
14.295	0.00193 46.27 0.95	1.00 E	0.00193 46.27 0.95	1.00 E	0.00193 46.27 0.95	1.00 E	0.00193 46.27 0.95	1.00 E
16.44	0.00157 60.6 0.712	1.98	0.00208 34.51 1.25	1.00 E	0.00208 34.51 1.25	1.00 E	0.00208 34.51 1.25	1.00 E
20.56	0.001093 99.1 0.414	4.54	0.00233 21.82 1.88	1.00 E	0.001992 29.97 1.37	1.37	0.00233 21.82 1.88	1.00 E
23.85	0.000809 153.64 0.247	10.33	0.00243 17.07 2.22	1.14	0.00147 46.48 0.817	3.13	0.0026 15.00 2.56	1.00 (E)
26.87	0.000629 224.9 0.16	19.39	0.001886 24.99 1.45	2.16	0.00114 68.04 0.534	5.90	0.00277 19.37 3.13	1.00 (E)
29.82	0.000487 336.6 0.104	36.44	0.00146 37.40 0.936	4.05	0.000885 101.83 0.344	11.04	0.00266 11.3 3.09	1.22
32.31	0.000389 484.8 0.069	61.88	0.00117 53.87 0.62	6.84	0.00071 146.6 0.23	18.57	0.00212 16.29 2.06	2.08

J_{dc} levels. θ_R is the diode thermal resistance that is required to limit the diode temperature rise to 225°C under CW conditions.

Table III presents the predicted CW performance for structure DR1 when thermal limitations are taken into account. Four combinations of heat sink material and diode geometry are considered. CM is for the case where a copper heat sink is used and where the diode is a single mesa structure; DM is the case of a diamond heat sink and diode single mesa structure; CR is the case with a copper heat sink, but where the diode has a ring geometry (or where multiple mesas are used to reduce the thermal resistance); and DR is the case with a diamond heat sink and diode ring geometry. The equations used to calculate the thermal resistance for each of these cases are explained in [4]. If a ring geometry or multiple mesa structure is used, it is assumed to reduce the spreading term in the thermal resistance expression by the factor 0.55.

In Table III, for the cases that are thermally limited, the values of D, θ, and P_{RF} given restrict the diode temperature rise to 225°C; R_c is the circuit resistance needed to match the diode negative resistance for these cases. If R_c based on thermal considerations becomes smaller than 1 Ω, it is assumed that the CW performance is electronically limited due to matching considerations; in these cases the data given in Table II are reproduced and an "E" is appended to denote that the operating point is electronically limited. It is seen that diode DR1 is not thermally limited up to $J_{dc} = 20.56$ kA/cm^2, provided diamond heat sinking is used.

Table IV presents the large-signal results obtained for structure DR3 along with power levels and required thermal resistances for the case of 1-Ω negative resistance. Comparison of Table IV with the results for the first structure DR1 given in Table II shows that at the same bias current level, e.g., $J_{dc} \cong 20$ kA/cm^2, both structures are generating comparable RF power when matched to 1 Ω; however, the dissipated power is higher and the required thermal resistance lower for structure DR1 due to its lower efficiency. If the devices are operated at the same efficiency level, e.g., using $J_{dc} = 16.44$ kA/cm^2 for DR1 and $J_{dc} = 49.5$ kA/cm^2 for DR3, structure DR3 is found to generate more power. Therefore, structure DR3 is preferred where thermal limitations are important. Also, it is capable of generating more power under pulsed conditions because the efficiency stays high for larger values of bias current.

Table V gives the CW performance for structure DR3 taking thermal limitations into account, which should be compared with Table III for structure DR1. For all combinations of heat sink material and diode geometry, structure DR3 can generate more CW power at 60 GHz.

Table VI gives the optimum efficiency results obtained at 60 GHz for five different hybrid structures that were studied. The dc solution for the starting structure H1 is shown in Fig. 3(a). This structure yielded very low efficiency and power output so no further data for H1 is presented. The efficiency of this structure can be significantly increased by raising the electric field on both sides; this has been accomplished in structure H2 by reducing

TABLE IV
LARGE-SIGNAL RESULTS VERSUS J_{dc} FOR STRUCTURE DR3 OF TABLE I
($f = 60$ GHz, $T = 500$ K)

J_{dc} (kA/cm^2)	$-Q_D$ (s/cm^2)	B_D (s/cm^2)	D (1 Ω) (inch)	V_{op} (V)	η (%)	P_{RF} (1 Ω) (W)	P_{diss} (1 Ω) (W)	θ_R (1 Ω) (°C/W)	V_{RF} (V)
15.0	642.25	6446.7	0.00174	20.45	22.0	1.03	3.66	61.52	14.5
17.64	738.76	6337.0	0.00189	20.41	21.57	1.41	5.12	43.95	14.5
19.98	836.6	6235.5	0.00204	20.5	21.48	1.86	6.8	33.08	14.5
24.00	999.8	6058.5	0.00229	20.64	21.25	2.78	10.36	21.73	14.5
28.25	1117.6	5861.7	0.00249	20.48	20.31	3.69	14.28	15.76	14.5
30.16	1175.89	5772.7	0.00259	20.47	20.02	4.19	16.73	13.45	14.5
32.1	1226.56	5682.5	0.00268	20.43	19.66	4.68	19.12	11.77	14.5
35.5	1303.5	5521.5	0.00283	20.3	18.98	5.55	24.05	9.35	14.5
39.9	1434.9	5307.2	0.00306	20.4	18.52	7.16	31.58	7.13	14.5
45.9	1505.6	5021.4	0.00329	20.1	17.11	8.67	41.88	5.37	14.5
49.5	1512.4	4857.2	0.0034	20.0	16.1	9.29	48.59	4.63	14.5

TABLE V
CW PERFORMANCE OF STRUCTURE DR3 OF TABLE I TAKING INTO ACCOUNT THERMAL LIMITATIONS
($f = 60$ GHz)

J_{dc} (kA/cm^2)	CM D (inch) θ (°C/W) P_{RF} (W)	CM R_c (Ω)	DM D (inch) θ (°C/W) P_{RF} (W)	DM R_c (Ω)	CR D (inch) θ (°C/W) P_{RF} (W)	CR R_c (Ω)	DR D (inch) θ (°C/W) P_{RF} (W)	DR R_c (Ω)
15.0	0.00174 61.52 1.03	1.00 (E)	0.00174 61.52 1.03	1.00 (E)	0.00174 61.52 1.03	1.00 (E)	0.00174 61.52 1.03	1.00 (E)
17.64	0.001691 54.96 1.125	1.25	0.00189 43.95 1.41	1.00 (E)	0.00189 43.95 1.41	1.00 (E)	0.00189 43.95 1.41	1.00 (E)
19.98	0.001394 71.1 0.865	2.14	0.00204 33.08 1.86	1.00 (E)	0.00204 33.08 1.86	1.00 (E)	0.00204 33.08 1.86	1.00 (E)
24.0	0.00102 109.7 0.553	5.04	0.00229 21.73 2.78	1.00 (E)	0.001853 33.18 1.83	1.53	0.00229 21.73 2.78	1.00 (E)
28.25	0.000743 174.3 0.329	11.23	0.002229 19.368 2.959	1.25	0.001351 52.73 1.087	3.40	0.00249 15.76 3.69	1.00 (E)
30.16	0.000664 216.74 0.26	15.21	0.001932 24.08 2.338	1.80	0.001171 65.56 0.86	4.89	0.00259 13.45 4.19	1.00 (E)
32.1	0.000557 271.82 0.203	23.15	0.00167 30.2 1.824	2.58	0.001013 82.22 0.67	7.00	0.00268 11.77 4.68	1.00 (E)
35.5	0.000426 418.2 0.126	44.0	0.00128 46.5 1.13	4.91	0.000774 126.5 0.416	13.3	0.00232 14.0 3.75	1.48

TABLE VI
LARGE-SIGNAL RESULTS AT 60 GHz FOR DIFFERENT HYBRID DOPING PROFILE PARAMETERS USING THE ENERGY-MOMENTUM SIMULATION
($N_D = 5.63 \times 10^{16}$ cm^{-3}, $T = 500$ K)

Case No.	ℓ_p (μm)	ℓ_n (μm)	w (μm)	N_A (10^{17} cm^{-3})	N_D^H (10^{17} cm^{-3})	V_{RF} (V)	V_{op} (V)	J_{dc} (kA/cm^2)	η (%)	Y_D (s/cm^2)	P_{RF} (10^4 W/cm^2)	P_{RF} (W) (R_D = 1 Ω)	P_{diss} (W) (R_D = 1 Ω)
H1	0.25	0.23	0.60	1.87	2.85	12.0	20.68	6.15	12.44	- 220.1 + j6803	1.585	0.075	0.529
H2	0.25	0.23	0.60	1.5	2.23	13.0	20.92	12.12	17.91	- 537.7 + j6517	4.544	0.571	2.62
H3	0.25	0.13	0.50	1.5	2.23	13.0	19.97	12.17	20.48	- 589.4 + j7668	4.98	0.496	1.926
H4	0.25	0.07	0.44	1.5	2.23	13.0	19.47	18.46	21.05	- 895.1 + j8210	7.56	0.992	3.724
H5	0.35	0.13	0.60	1.0	2.23	14.5	21.52	16.0	20.78	- 685.4 + j6342	7.205	1.214	4.594

both N_A and N_D^H. In structure H3 and H4, the efficiency is further increased by reducing the length of the n-drift region l_n while keeping l_p constant. Although the highest efficiency was obtained in this manner, overall the best structure was found to be H5. H5 has the same total length as the starting structure H1, but 0.1 μm has been subtracted from l_n and added to l_p. Since l_p is larger, N_A is further reduced so that the electric field at the left-hand contact is not too low. Increasing l_p has very little effect on the efficiency; however, the power available when matching to 1-Ω circuit resistance is greater than for H3 or H4 since structure H5 is longer. This reduces the susceptance

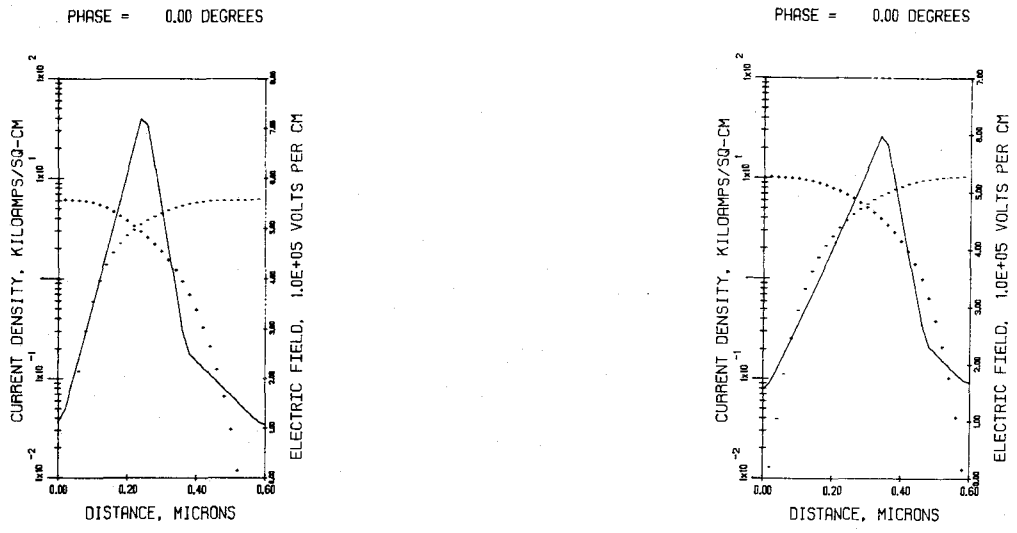

Fig. 3. (a) DC solution for structure H1 of Table VI ($J_{dc} = 6$ kA/cm^2, $T = 500$ K, $V_{dc} = 20.51$ V) and (b) dc solution for structure H5 ($J_{dc} = 10$ kA/cm^2, $T = 500$ K, $V_{dc} = 20.5$ V).

TABLE VII
LARGE-SIGNAL RESULTS VERSUS J_{dc} FOR STRUCTURE H5 OF TABLE VI
($f = 60$ GHz, $T = 500$ K)

J_{dc} (kA/cm^2)	$-G_D$ (s/cm^2)	B_D (s/cm^2)	D (1 Ω) (inch)	V_{op} (V)	η (%)	P_{RF} (1 Ω) (W)	P_{diss} (1 Ω) (W)	θ_R (1 Ω) (°C/W)	V_{RF} (V)
10.0	418.7	6620	0.00137	21.43	20.36	0.419	1.621	138.8	14.5
12.04	510.0	6530	0.00153	21.52	20.68	0.637	2.44	92.07	14.5
14.0	596.0	6439	0.00165	21.55	20.77	0.868	3.314	67.9	14.5
16.06	685.4	6342	0.00182	21.59	20.78	1.214	4.626	48.64	14.5
18.04	767.7	6250	0.00196	21.61	20.7	1.562	5.98	37.64	14.5
20.06	849.6	6156	0.00208	21.62	20.6	1.964	7.58	29.7	14.5
25.16	1046	5918	0.00239	21.62	20.2	3.186	12.57	17.9	14.5
29.53	1193	5713	0.00263	21.54	19.71	4.39	17.89	12.58	14.5
39.48	1496	5249	0.00315	21.37	18.63	7.89	35.54	6.33	14.5
48.91	1753	4823	0.00362	21.24	17.73	12.27	56.88	3.96	14.5
60.36	1971	4330	0.00415	20.92	16.4	18.04	91.9	2.45	14.5

for H5 and allows a bigger diode area. Structure H5 is also capable of generating more CW power than any of the other structures when thermal limitations are considered. The dc solution for structure H5 is shown in Fig. 3(b).

Table VII presents the large-signal results obtained for structure H5 at $f = 60$ GHz and the power obtainable if the diode is matched to 1-Ω circuit resistance, and Table VIII gives the predicted CW performance taking thermal limitations into account. Comparison of these tables with the corresponding tables for DR1 and DR3 shows that the hybrid is comparable to the double-read in efficiency and slightly better in expected CW power output at $f = 60$ GHz. In addition, the hybrid can be operated at higher bias currents and at higher peak power than the double-read for pulsed applications, e.g., comparison of Tables VII and IV shows that, at $J_{dc} = 60$ kA/cm^2, the hybrid H5 is operating with an efficiency of $\eta = 16.4$ percent and generating 18 W while the double-read structure DR3 has dropped to 16.1-percent efficiency at $J_{dc} = 50$ kA/cm^2 and is generating 9.3 W RF power.

III. RESULTS AT 94 GHz

Table IX gives the optimum efficiency results obtained for two double-read structures simulated at 94 GHz. Structure DR2 was obtained from DR1 by shortening the electron drift region l_n which resulted in higher efficiency. Fig. 4(a) shows the dc solution of the starting structure

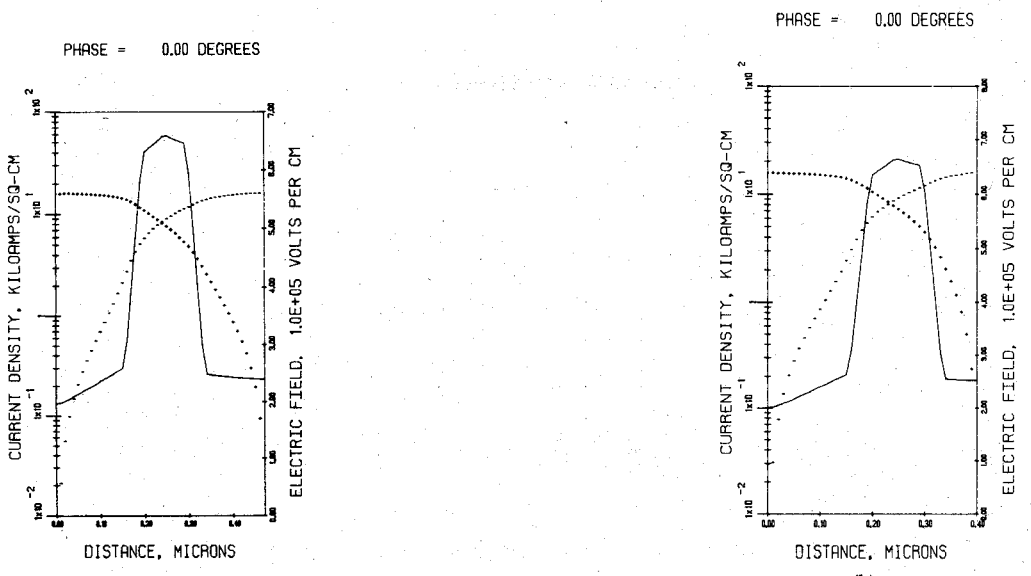

Fig. 4. (a) DC solution for structure DR1 of Table IX ($J_{dc}=16$ kA/cm^2, $T=500$ K, $V_{dc}=16.8$ V) and (b) dc solution for structure DR2 of Table IX ($J_{dc}=16$ kA/cm^2, $T=500$ K, $V_{dc}=15.42$ V).

TABLE VIII
CW PERFORMANCE OF STRUCTURE H5 OF TABLE VI TAKING INTO ACCOUNT THERMAL LIMITATIONS
($f=60$ GHz)

J_{dc} (kA/cm^2)	CM D (inch) θ (°C/W) P_{RF} (W)	CM R_c (Ω)	DM D (inch) θ (°C/W) P_{RF} (W)	DM R_c (Ω)	CR D (inch) θ (°C/W) P_{RF} (W)	CR R_c (Ω)	DR D (inch) θ (°C/W) P_{RF} (W)	DR R_c (Ω)
16.06	0.00176 52.18 1.13	1.07	0.00182 48.64 1.21	1.00 (E)	0.00182 48.64 1.21	1.00 (E)	0.00182 48.64 1.21	1.00 (E)
18.04	0.00148 65.6 0.895	1.75	0.00196 37.64 1.56	1.00 (E)	0.00196 37.64 1.56	1.00 (E)	0.00196 37.64 1.56	1.00 (E)
20.06	0.00125 82.36 0.708	2.78	0.00208 29.7 1.96	1.00 (E)	0.00208 29.7 1.96	1.00 (E)	0.00208 29.7 1.96	1.00 (E)
25.16	0.000837 146 0.39	8.15	0.00239 17.9 3.19	1.00 (E)	0.00152 44.18 1.29	2.47	0.00239 17.9 3.19	1.00 (E)
29.53	0.000597 243.5 0.227	19.41	0.00179 27.05 2.04	2.16	0.00109 73.65 0.75	5.86	0.00263 12.58 4.39	1.00 (E)
39.48	0.000251 1026 0.05	158	0.000753 114 0.452	17.5	0.000456 310.3 0.166	47.7	0.00137 34.47 1.49	5.29

TABLE IX
LARGE-SIGNAL RESULTS AT 94 GHz FOR DIFFERENT DOUBLE-READ DOPING PROFILE PARAMETERS USING THE ENERGY-MOMENTUM SIMULATION
($N_A=5\times10^{16}$ cm^{-3}, $N_D=2.5\times10^{16}$ cm^{-3}, $T=500$ K)

Case No.	ℓ_p (μm)	ℓ_n (μm)	w (μm)	Q_p (10^{12} cm^{-2})	Q_n (10^{12} cm^{-2})	V_{RF} (V)	V_{op} (V)	J_{dc} (kA/cm^2)	η (%)	Y_D (s/cm^2)	P_{RF} (W/cm^2)	P_{RF} (W) (R_D = 1 Ω)	P_{diss} (W) (R_D= 1 Ω)
DR1	0.175	0.155	0.47	2.6	2.8	11	17.87	36.5	15.06	- 1.626 x 10^3 + j1.35 x 10^4	9.835 x 10^4	0.87	4.87
DR2	0.24	0.085	0.40	2.6	2.8	11	17.32	29.65	18.00	- 1.529 x 10^3 + j1.568 x 10^4	9.249 x 10^4	0.57	2.59

TABLE X
LARGE-SIGNAL RESULTS FOR STRUCTURE DR1 OF TABLE IX
($f = 94$ GHz, $T = 500$ K)

J_{dc} (kA/cm^2)	$-G_D$ (s/cm^2)	B_D (s/cm^2)	D (1 Ω) (inch)	V_{op} (V)	η (%)	P_{RF} (1 Ω) (W)	P_{diss} (1 Ω) (W)	θ_R (1 Ω) (°C/W)	V_{RF} (V)
15.84	656	13,850	0.00082	17.34	14.44	0.14	0.8	281.25	11
20.05	857	13,790	0.00094	17.48	14.78	0.23	1.35	167.0	11
24.3	1056	13,720	0.00105	17.59	14.94	0.35	2.02	111.59	11
28.46	1251	13,660	0.00115	17.69	15.02	0.5	2.85	79.03	11
32.5	1438	13,580	0.00123	17.78	15.05	0.67	3.79	59.38	11
36.5	1626	13,500	0.00132	17.87	15.06	0.87	4.87	46.16	11
42.8	1915	13,360	0.00144	17.99	15.05	1.22	6.87	32.75	11
48.8	2184	13,220	0.00155	18.1	14.96	1.61	9.14	24.61	11
55.9	2496	13,030	0.00167	18.2	14.83	2.14	12.29	18.31	11
62.98	2788	12,820	0.00179	18.3	14.65	2.73	15.93	14.12	11
71.1	3109	12,570	0.00191	18.35	14.42	3.49	20.71	10.86	11
81.1	3476	12,220	0.00206	18.42	14.1	4.53	27.62	8.15	11

TABLE XI
CW PERFORMANCE OF STRUCTURE DR1 OF TABLE IX TAKING INTO ACCOUNT THERMAL LIMITATIONS
($f = 94$ GHz)

J_{dc} (kA/cm^2)	CM D (inch) θ (°C/W) P_{RF} (W)	CM R_c (Ω)	DM D (inch) θ (°C/W) P_{RF} (W)	DM R_c (Ω)	CR D (inch) θ (°C/W) P_{RF} (W)	CR R_c (Ω)	DR D (inch) θ (°C/W) P_{RF} (W)	DR R_c (Ω)
24.3	0.00105 111.6 0.35	1.00 (E)	0.00105 111.6 0.35	1.00 (E)	0.00105 111.6 0.35	1.00 (E)	0.00105 111.6 0.35	1.00 (E)
28.46	0.000913 124.4 0.32	1.59	0.00115 79.03 0.50	1.00 (E)	0.00115 79.03 0.50	1.00 (E)	0.00115 79.03 0.50	1.00 (E)
32.5	0.000706 181.4 0.22	3.03	0.00123 59.38 0.67	1.00 (E)	0.00123 59.38 0.67	1.00 (E)	0.00123 59.38 0.67	1.00 (E)
36.5	0.000544 270.3 0.148	5.33	0.00132 46.16 0.87	1.00 (E)	0.00099 8.18 0.488	1.78	0.00132 46.16 0.87	1.00 (E)
42.8	0.000355 538.1 0.074	16.45	0.00106 59.8 0.67	1.83	0.000646 163 0.245	4.97	0.00144 32.8 1.22	1.00 (E)
48.8	0.000219 1236 0.032	50.1	0.000656 137 0.288	5.58	0.000398 374 0.106	15.17	0.00119 41.5 0.953	1.70
55.9	0.000096 5594 0.007	303	0.000287 622 0.063	33.9	0.000174 1692 0.023	92.1	0.000522 188 0.208	9.15

DR1 and Fig. 4(b) shows the dc solution for the shorter structure DR2.

Table X presents the large-signal results obtained at $f = 94$ GHz for DR1 and the power obtainable if the diode is matched to 1-Ω circuit resistance, and Table XI gives the predicted CW performance for this device. Table XII presents the large-signal results for structure DR2 at $f = 94$ GHz, and Table XIII gives the predicted CW performance for DR2. Comparison of Tables X and XII shows that both devices generate comparable RF power when matched to the same resistance level, provided thermal limitations are not important. However, comparison of Tables XI and XIII shows that structure DR2 can generate more power under CW conditions due to the higher efficiency.

Table XIV presents optimum efficiency results obtained for two different hybrid profiles at 94 GHz. Both profiles are 0.4 μm long; however, the n-drift region for structure H2 is shorter and the p-drift region correspondingly longer than for structure H1. Also, the doping levels N_A and N_D^H were modified in structure H2 to bring the electric field down to approximately the same values at the contacts as for structure H1. Fig. 5(a) shows the dc solution for

TABLE XII
LARGE-SIGNAL RESULTS FOR STRUCTURE DR2 OF TABLE IX
($f = 94$ GHz, $T = 500$ K)

J_{dc} (kA/cm^2)	$-G_D$ (s/cm^2)	B_D (s/cm^2)	D (1 Ω) (inch)	V_{op} (V)	η (%)	P_{RF} (1 Ω) (W)	P_{diss} (1 Ω) (W)	θ_R (1 Ω) (°C/W)	V_{RF} (V)
16.15	786	16,088	0.00077	16.8	17.51	0.14	0.7	321.0	11
20.1	1015	15,971	0.00088	17.03	17.93	0.24	1.12	200.46	11
24.5	1247	15,843	0.00099	17.16	17.96	0.37	1.69	133.2	11
29.65	1529	15,679	0.0011	17.32	18.00	0.56	2.56	87.93	11
34.9	1812	15,504	0.00121	17.46	17.98	0.82	3.72	60.45	11
40.05	2087	15,323	0.00131	17.59	17.91	1.1	5.04	44.64	11
45.12	2352	15,137	0.00141	17.71	17.81	1.43	6.58	34.18	11
50.14	2611	14,945	0.0015	17.8	17.69	1.79	8.33	27.02	11
55.13	2862	14,744	0.00158	17.88	17.65	2.20	10.12	22.22	11
60.08	3106	14,536	0.00167	17.95	17.42	2.64	12.52	17.97	11
70.00	3569	14,096	0.00183	18.07	17.08	3.65	17.7	12.71	11
75.00	3788	13,862	0.0019	18.1	16.90	4.2	24.69	9.11	11
87.1	4386	13,278	0.0021	18.29	16.65	5.94	29.8	7.55	11
96.15	4730	12,815	0.00224	18.31	16.25	7.28	37.32	6.03	11
99.00	4759	12,644	0.00227	18.22	15.96	7.46	39.44	5.71	11

TABLE XIII
CW PERFORMANCE OF STRUCTURE DR2 OF TABLE IX TAKING INTO ACCOUNT THERMAL LIMITATIONS
($f = 94$ GHz)

J_{dc} (kA/cm^2)	CM D (inch) θ (°C/W) P_{RF} (W)	CM R_c (Ω)	DM D (inch) θ (°C/W) P_{RF} (W)	DM R_c (Ω)	CR D (inch) θ (°C/W) P_{RF} (W)	CR R_c (Ω)	DR D (inch) θ (°C/W) P_{RF} (W)	DR R_c (Ω)
24.5	0.00099 133 0.37	1.00 (E)	0.00099 133 0.37	1.00 (E)	0.00099 133 0.37	1.00 (E)	0.00099 133 0.37	1.00 (E)
29.6	0.000939 120 0.413	1.37	0.00110 87.9 0.56	1.00 (E)	0.00110 87.9 0.56	1.00 (E)	0.00110 87.9 0.56	1.00 (E)
34.9	0.00068 192 0.257	3.17	0.00121 60.4 0.82	1.00 (E)	0.00121 60.4 0.82	1.00 (E)	0.00121 60.4 0.82	1.00 (E)
40.0	0.00049 316 0.155	7.15	0.00131 44.6 1.10	1.00 (E)	0.000896 95.5 0.514	2.14	0.00131 44.6 1.10	1.00 (E)
45.1	0.00035 548 0.089	16.2	0.00105 60.9 0.80	1.8	0.000638 166 0.294	4.88	0.00141 34.2 1.43	1.00 (E)
50.1	0.000239 1055 0.046	39.4	0.000718 117 0.413	4.36	0.000435 319 0.152	11.9	0.001305 35.5 1.36	1.32
55.1	0.000149 2468 0.019	112	0.000446 274 0.175	12.6	0.00027 746 0.064	34.2	0.000812 82.9 0.578	3.79

structure H1 and Fig. 5(b) gives the dc solution for structure H2. Table XV presents large-signal results at 94 GHz obtained for structure H1 and Table XVI gives the predicted CW performance of H1 at 94 GHz. Table XVII gives the large-signal results for structure H2 of Table XIV and Table XVIII gives the predicted CW performance for structure H2 at 94 GHz.

Comparison of Tables XV and XVII shows that the hybrid structure H2 generates more power than H1 when both are matched to 1-Ω circuit resistance. This is because the efficiency is higher for H2 and the overall device lengths are the same. Also, comparison of Tables XVI and XVIII shows that structure H2 can generate more CW power than H1 at 94 GHz for all combinations of heat sink

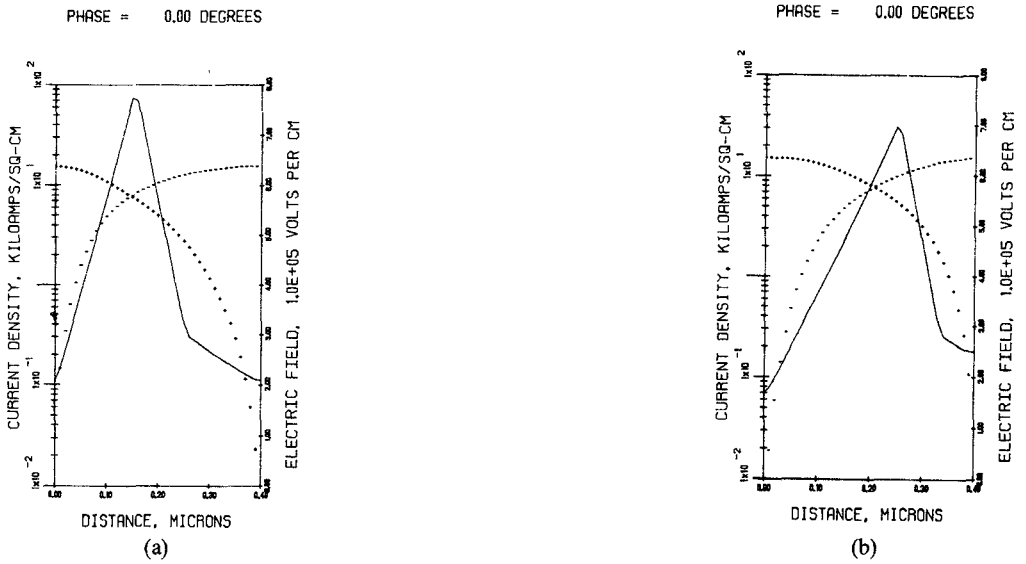

Fig. 5. (a) DC solution for structure H1 of Table XIV ($J_{dc}=15$ kA/cm^2, $T=500$ K, $V_{dc}=16.6$ V) and (b) dc solution for structure H2 ($J_{dc}=15$ kA/cm^2, $T=500$ K, $V_{dc}=17.1$ V).

TABLE XIV
LARGE-SIGNAL RESULTS AT 94 GHz FOR DIFFERENT HYBRID DOPING PROFILE PARAMETERS USING THE ENERGY-MOMENTUM SIMULATION
($N_D=6.6\times10^{16}$ cm^{-3}, $T=500$ K)

Case No.	ℓ_p (μm)	ℓ_n (μm)	w (μm)	N_A (10^{17} cm^{-3})	N_D^H (10^{17} cm^{-3})	V_{RF} (V)	V_{op} (V)	J_{dc} (kA/cm^2)	η (%)	Y_D (s/cm^2)	P_{RF} (10^4 W/cm^2)	P_{RF} (W) (R_D = 1 Ω)	P_{diss} (W) (R_D = 1 Ω)
H1	0.16	0.14	0.4	1.8	3.8	11	17.49	30	15.51	-1341 + j15,555	8.11	0.446	2.428
H2	0.25	0.05	0.4	1.3	3.9	11.5	18.32	30.0	18.4	-1531 + j15,445	10.1	0.64	2.85

TABLE XV
LARGE-SIGNAL RESULTS FOR STRUCTURE H1 OF TABLE XIV
($f=94$ GHz, $T=500$ K)

J_{dc} (kA/cm^2)	$-G_D$ (s/cm^2)	B_D (s/cm^2)	D (1 Ω) (inch)	V_{op} (V)	η (%)	P_{RF} (1 Ω) (W)	P_{diss} (1 Ω) (W)	θ_R (1 Ω) (°C/W)	V_{RF} (V)
15	676	16,044	0.00072	17.42	15.49	0.107	0.578	389.39	11
19.83	878	15,892	0.00083	17.4	15.4	0.184	1.012	222.37	11
24.88	1109	15,724	0.00094	17.44	15.45	0.3	1.633	137.7	11
30	1341	15,555	0.001042	17.49	15.51	0.446	2.428	92.67	11
34.88	1557	15,380	0.001134	17.5	15.42	0.518	2.839	79.26	11
38.16	1688	15,261	0.001189	17.48	15.3	0.73	4.046	55.6	11
44.8	1973	15,021	0.0013	17.52	15.2	1.02	5.73	39.29	11
50.48	2188	14,803	0.00139	17.48	15.0	1.29	7.33	30.71	11
54.64	2374	14,651	0.00146	17.52	15.0	1.54	8.78	25.63	11
62.24	2655	14,345	0.00157	17.5	14.74	2.00	12.74	17.67	11
67.16	2781	14,154	0.00162	17.42	14.38	2.25	13.39	16.8	11

TABLE XVI
CW PERFORMANCE OF STRUCTURE H1 OF TABLE XIV TAKING INTO ACCOUNT THERMAL LIMITATIONS
($f = 94$ GHz)

J_{dc} (kA/cm^2)	CM D (inch) θ (^{o}C/W) P_{RF} (W)	CM R_c (Ω)	DM D (inch) θ (^{o}C/W) P_{RF} (W)	DM R_c (Ω)	CR D (inch) θ (^{o}C/W) P_{RF} (W)	CR R_c (Ω)	DR D (inch) θ (^{o}C/W) P_{RF} (W)	DR R_c (Ω)
24.9	0.00094 138 0.30	1.00 (E)	0.00094 138 0.30	1.00 (E)	0.00094 138 0.30	1.00 (E)	0.00094 138 0.30	1.00 (E)
29.9	0.000906 122 0.34	1.32	0.00104 92.7 0.446	1.00 (E)	0.00104 92.7 0.446	1.00 (E)	0.00104 92.7 0.446	1.00 (E)
34.9	0.00068 186 0.22	2.78	0.00113 79.3 0.518	1.00 (E)	0.00113 79.3 0.518	1.00 (E)	0.00113 79.3 0.518	1.00 (E)
38.2	0.000564 246 0.165	4.44	0.00119 55.6 0.73	1.00 (E)	0.00103 74.6 0.545	1.33	0.00119 55.6 0.73	1.00 (E)
44.8	0.00038 460 0.088	11.7	0.00114 51.1 0.79	1.30	0.00069 139 0.29	3.55	0.0013 39.3 1.02	1.00 (E)
50.5	0.000263 855 0.046	27.9	0.000789 95.0 0.418	3.1	0.000478 259 0.153	8.46	0.00139 30.7 1.29	1.00 (E)
54.6	0.000191 1490 0.0265	58.4	0.000573 166 0.239	6.49	0.000347 452 0.088	17.7	0.00104 50.3 0.79	1.97

TABLE XVII
LARGE-SIGNAL RESULTS FOR STRUCTURE H2 OF TABLE XIV
($f = 94$ GHz, $T = 500$ K)

J_{dc} (kA/cm^2)	$-G_D$ (s/cm^2)	B_D (s/cm^2)	D (1 Ω) (inch)	V_{op} (V)	η (%)	P_{RF} (1 Ω) (W)	P_{diss} (1 Ω) (W)	θ_R (1 Ω) (^{o}C/W)	V_{RF} (V)
14.6	734	15,971	0.00075	18.26	18.18	0.14	0.63	357.14	11.5
20.2	1031	15,782	0.0009	18.29	18.4	0.28	1.25	180.16	11.5
24.5	1238	15,638	0.001	18.26	18.3	0.41	1.84	122.4	11.5
30.0	1531	15,445	0.00112	18.32	18.4	0.64	2.85	79.00	11.5
34.6	1716	15,289	0.0012	18.17	18.07	0.82	3.74	60.23	11.5
39.4	1946	15,091	0.00129	18.17	17.99	1.08	5.12	43.95	11.5
48.6	2366	14,743	0.00145	18.14	17.75	1.66	7.69	29.26	11.5
58.8	2824	14,342	0.00162	18.13	17.51	2.47	11.51	19.53	11.5
68.4	3230	13,956	0.00176	18.12	17.22	3.36	16.16	13.93	11.5
78.4	3639	13,548	0.00191	18.12	16.92	4.46	21.81	10.31	11.5
88.4	4018	13,138	0.00205	18.1	16.6	5.66	28.4	7.92	11.5
98.4	4370	12,724	0.00218	18.07	16.26	6.98	35.95	6.26	11.5
108	4698	12,310	0.00231	18.3	15.89	8.42	45.26	4.97	11.5
118	4999	11,896	0.00243	17.98	15.52	9.94	53.97	4.17	11.5
128	5276	11,484	0.00255	17.94	15.14	11.49	64.66	3.48	11.5

material and diode geometry. Comparing the results for H2 with those of the double-read structures DR1 and DR2 in Table IX shows that the hybrid structure H2 can generate power comparable to that of a double-read structure at 94 GHz, both under CW conditions and when matched to 1-Ω circuit resistance.

IV. CONCLUSIONS

Hybrid and double-read structures have been simulated and compared at 60 and 94 GHz using the energy-momentum transport model. It is found that best efficiency and power output are obtained using electron drift region

TABLE XVIII
CW PERFORMANCE OF STRUCTURE H2 OF TABLE XIV TAKING INTO ACCOUNT THERMAL LIMITATIONS
(f = 94 GHz)

J_{dc} (kA/cm^2)	CM D (inch) θ (°C/W) P_{RF} (W)	CM R_c (Ω)	DM D (inch) θ (°C/W) P_{RF} (W)	DM R_c (Ω)	CR D (inch) θ (°C/W) P_{RF} (W)	CR R_c (Ω)	DR D (inch) θ (°C/W) P_{RF} (W)	DR R_c (Ω)
24.5	0.001 122 0.41	1.00 (E)	0.001 122 0.41	1.00 (E)	0.001 122 0.41	1.00 (E)	0.001 122 0.41	1.00 (E)
30.0	0.00839 141 0.361	1.78	0.00112 79.0 0.64	1.00 (E)	0.00112 79.0 0.64	1.00 (E)	0.00112 79.0 0.64	1.00 (E)
34.6	0.00639 211 0.235	3.53	0.0012 60.2 0.82	1.00 (E)	0.00116 63.8 0.778	1.06	0.0012 60.2 0.82	1.00 (E)
39.4	0.000474 336 0.147	7.41	0.00129 44.0 1.08	1.00 (E)	0.000863 102 0.485	2.23	0.00129 44.0 1.08	1.00 (E)
48.6	0.000249 985 0.049	33.91	0.000748 109 0.444	3.76	0.000454 298 0.163	10.20	0.00136 33.1 1.47	1.14
58.8	0.000082 7550 0.006	390	0.000245 839 0.057	43.7	0.000149 2280 0.021	118	0.000446 253 0.188	13.2

lengths considerably shorter than is predicted by conventional IMPATT theory. Also, more power is obtained if the hole drift region is longer than the electron drift region since increasing the hole drift region does not seriously degrade the device efficiency, but the increased length allows a larger diode area when matching to a particular circuit resistance level. For the structures that were studied, the hybrid performance was comparable to, and in some cases better than that of, the double-read structures so that there does not appear to be any compelling reason to use the double-read structure at 60 and 94 GHz.

REFERENCES

[1] R. K. Mains, G. I. Haddad, and P. A. Blakey, "Simulation of GaAs IMPATT diodes including energy and velocity transport equations," *IEEE Trans. Electron Devices*, vol. ED-30, no. 10, Oct. 1983.

[2] R. K. Mains, M. El-Gabaly, G. I. Haddad, and J. P. Sun, "Comparison of theoretical and experimental results for millimeter-wave GaAs IMPATT's," *IEEE Trans. Electron Devices*, vol. ED-31, no. 9, pp. 1273–1279, Sept. 1984.

[3] M. El-Gabaly, R. K. Mains, and G. I. Haddad, "Effects of doping profile on GaAs double-drift IMPATT diodes at 33 and 44 GHz using the energy-momentum transport model," *IEEE Trans. Microwave Theory Tech.*, vol. MTT-32, pp. 1353–1361, Oct. 1984.

[4] R. K. Mains and G. I. Haddad, "Properties and capabilities of millimeter-wave IMPATT diodes," in *Infrared and Millimeter Waves*, K. J. Button, Ed., vol. 10. New York: Academic Press.

Moustafa A. El-Gabaly (S'70–M'74–SM'81) received the B.Sc. degree in electrical engineering and the B.Sc. degree in mathematics from the University of Cairo, Egypt, in 1965 and 1969, respectively. He received the Ph.D. degree in electrical engineering from the University of Alberta, Canada, in 1974.

During 1974 and 1975, he was with AGT, Canada, as a Design Microwave Systems Engineer. In 1976, he joined the faculty of the University of Kuwait, where he now an Associate Professor of Electrical Engineering. He also serves as a technical consultant at Kuwait Institute of Scientific Research. During the summers of 1977 to 1980, he was a Visiting Research Scientist at the Electron Physics Laboratory, the University of Michigan, Ann Arbor. Since April 1983, he has been a Visiting Associate Professor in the Department of Electrical and Computer Engineering, the University of Michigan. His research area includes microwave solid-state devices, photovoltaic energy conversion, and photoelectronic properties of crystalline and amorphous semiconductors.

Dr. El-Gabaly received the Government of Alberta Fellowship and the National Research Council of Canada Fellowship in 1972 and 1973, respectively. He is a Professional Engineer, registered in the Province of Alberta, Canada, and is a member of the International Solar Energy Society (ISES).

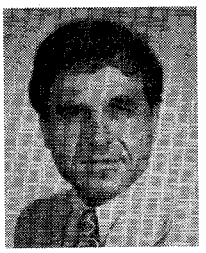

George I. Haddad (S'57–M'61–SM'66–F'72) was born in Aindara, Lebanon, on April 7, 1935. He received the B.S.E., M.S.E., and Ph.D. degrees in electrical engineering in 1956, 1958, and 1963, respectively, from the University of Michigan, Ann Arbor.

From 1957 to 1958, he was associated with the Engineering Research Institute of the University of Michigan, where he was engaged in research of electromagnetic accelerators. In 1958, he joined the Electron Physics Laboratory, University of Michigan, where he has been engaged in research of masers and parametric devices. He held a University of Michigan Research Institute Fellowship for the academic year of 1958–1959 and a Sponsored Fellowship for the spring semester of 1959–1960. He served successively as Instructor, Assistant Professor, and Associate Professor in the Department of Electrical Engineering from 1960 to 1969. He is presently a Professor and Chairman of the Department of Electrical and Computer Engineering.

Dr. Haddad received the 1970 Curtis W. McGraw Research Award of the American Society of Engineering Education for outstanding achievements as an Engineering Teacher. He is a member of Eta Kappa Nu, Sigma, Xi, Phi, Kappa Phi, the American Physical Society, and the American Society for Engineering Education.

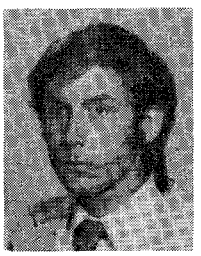

Richard K. Mains (S'79–M'79) was born in Chicago, IL, on March 28, 1950. He received the M.Sc. degree in electrical engineering in 1974 from Ohio State University, Columbus, and the Ph.D. degree in electrical engineering in 1979 from the University of Michigan, Ann Arbor.

At present, he is an assistant Research Scientist in the Electron Physics Laboratory, the University of Michigan.